Fission properties of superheavy nuclei for *r*-process calculations

Samuel A. Giuliani,[1,*] Gabriel Martínez-Pinedo,[1,2,†] and Luis M. Robledo[3,‡]

[1]*Institut für Kernphysik (Theoriezentrum), Technische Universität Darmstadt, Schlossgartenstraße 2, 64289 Darmstadt, Germany*

[2]*GSI Helmholtzzentrum für Schwerionenforschung, Planckstraße 1, 64291 Darmstadt, Germany*

[3]*Departamento de Física Teórica, Universidad Autónoma de Madrid, E-28049 Madrid, Spain*

(Received 4 April 2017; revised manuscript received 18 December 2017; published 26 March 2018)

We computed a new set of static fission properties suited for *r*-process calculations. The potential energy surfaces and collective inertias of 3640 nuclei in the superheavy region are obtained from self-consistent mean-field calculations using the Barcelona-Catania-Paris-Madrid energy density functional. The fission path is computed as a function of the quadrupole moment by minimizing the potential energy and exploring octupole and hexadecapole deformations. The spontaneous fission lifetimes are evaluated employing different schemes for the collective inertias and vibrational energy corrections. This allows us to explore the sensitivity of the lifetimes to those quantities together with the collective ground-state energy along the superheavy landscape. We computed neutron-induced stellar reaction rates relevant for *r*-process nucleosynthesis using the Hauser-Feshbach statistical approach and study the impact of collective inertias. The competition between different reaction channels including neutron-induced rates, spontaneous fission, and α decay is discussed for typical *r*-process conditions.

DOI: 10.1103/PhysRevC.97.034323

I. INTRODUCTION

The theoretical description of the fission process is one of the most challenging and fascinating problems in nuclear physics. The competition between the long-range Coulomb repulsion and the short-range strong interaction drives the evolution of the nucleus from the ground state to the scission point. Furthermore, they produce quantum mechanical shell effects that allow for the stability of superheavy (SH) elements in the heaviest regions of the nuclear landscape. Arguably one of the most interesting applications of fission concerns the *r*-process nucleosynthesis of superheavy elements. In scenarios with high neutron densities, such as the dynamical ejecta of neutron stars mergers, the competition between rapid neutron captures and β decays of seed nuclei leads to the synthesis of superheavy elements. The *r*-process path proceeds toward regions of unstable nuclei that undergo fission, recycling the material to lighter fission products [1–3]. In these conditions, fission plays a relevant role not only by modifying the final shape of the *r*-process abundances [4,5], but also in providing a mechanism to achieve a robust *r* process [6]. Besides astrophysical applications, the stability of the nucleus against fission is also crucial for the experimental synthesis of superheavy nuclei achieved in laboratories all around the world during the past years [7–10] and for energy production in nuclear reactors.

Nowadays, the main nuclear structure models describing the spontaneous fission (SF) are the microscopic-macroscopic (MicMac) and the self-consistent mean-field (SCMF) models (see Ref. [11] for a recent review on fission properties of SH nuclei covering MicMac and SCMF models). The MicMac description pioneered the modern modeling of the fission process in the late 1960s and since then several studies have been successfully applied in systematic calculations of superheavy nuclei. One of the main advantages of this method is the calculation of the potential energy surface in multidimensional spaces using up to five collective degrees of freedom for systematic calculations, providing an accurate description of multiple fission paths (see, e.g. Refs. [12–14] for recent calculations). On the other hand, 20 years ago fission calculations based on self-consistent methods with effective interactions entered the scene, proposing an alternative scheme built on a more microscopic approach. Starting from an effective energy density functional (EDF), the constrained Hartree-Fock (HF) and Hartree-Fock-Bogoliubov (HFB) theories permit the calculation of the fission properties rooted on more microscopic input. In recent years, several studies explored the capability of the EDF theory to reproduce the experimental fission data using either Skyrme [15–21], Gogny [22–28], or relativistic interactions [29] (see Ref. [30] for a complete review).

The main objective of this paper is to present the fission properties of *r*-process nuclei obtained with the Barcelona-Catania-Paris-Madrid (BCPM) EDF [31]. As already pointed out in Ref. [32], nowadays only few global calculations suited for *r*-process calculations are publicly available. This work is designed to provide a new set of fission properties based in the SCMF model covering the whole superheavy landscape and including nuclei with an odd number of protons and/or neutrons. The main advantage of the EDF theory is that it allows the computation of both the potential energy surface and the collective inertias from a unique and microscopic footing, providing a robust framework for the calculation of

*Present address: NSCL/FRIB Laboratory, Michigan State University, East Lansing, Michigan 48824, USA; giuliani@nscl.msu.edu

†g.martinez@gsi.de

‡luis.robledo@uam.es

spontaneous fission lifetimes, fission barrier heights, and isomer excitation energies. The paper is outlined as follows. In Sec. II we briefly introduce the method used in the calculation of the potential energy surface and spontaneous fission lifetimes. In Sec. III we summarize the results of our calculations. We start discussing the benchmark of BCPM against the experimental data in Sec. III A. The systematic of fission barriers and spontaneous fission lifetimes is discussed in Sec. III B and Sec. III C. Section III D is devoted to discussing the competition between α decay and spontaneous fission and in Sec. III E the discussion is extended to neutron-induced rates of relevance to the r process. Finally, in Sec. IV we summarize our results and outline the future perspectives.

II. METHODS

In this paper fission is described within the self-consistent mean-field (SCMF) approach [33] following the traditional HFB theory with constraining operators as described in Ref. [34]. For completeness we will summarize here the general computational scheme and point out the uncertainties arising from our method.

In order to reduce the computational cost, axial symmetry has been preserved in all the calculations. The impact of releasing this restriction has been the object of several recent studies (see, e.g., Refs. [19,20,26]), where it has been shown that triaxiality can reduce the inner fission barrier height of actinides up to 2–3 MeV. However, we would like to point out here that the role of triaxiality in fission is still the subject of discussion since some recent calculations showed that axial symmetry can be fully restored in dynamic calculations of the fission process [24,35,36]. Moreover, this reduction of the fission barrier is compensated by an increase of the collective inertias and therefore the impact of releasing this symmetry is expected to be small in the calculation of fission lifetimes.

Due to the preservation of axial symmetry, the mean value of the multipole operators, $\langle \boldsymbol{Q}_{\mu\nu} \rangle = 0$ for all $\nu \neq 0$. In order to explore the impact of octupole and hexadecapole deformations, as well as asymmetric fission, reflection symmetry is allowed to break at any stage of the calculations. The basis quantum numbers are restricted by the condition:

$$2n_\perp + |m| + \frac{n_z}{q} \leqslant N^{\max}. \tag{1}$$

All the calculations were carried with $N^{\max} = 17$ and $q = 3/2$. The parameter q represents the ratio of the number of quanta along the z direction to the number of quanta along the perpendicular one. The value used favors more shells in the z direction as required in fission. Once the number of quanta in each direction is fixed, the basis only depends on the oscillator lengths b_z and $b_\perp$. To diminish the impact of the limited basis size on the binding energies, it is mandatory to carefully optimize the oscillator length parameters for each value of the constrained quadrupole moment considered in the calculation [37]. The optimization is carried out automatically for all the nuclei using the gradient method to find the minimum of the HFB energy as a function of the two oscillator length variables $b_\perp$ and b_z. The gradient of the energy with respect to $b_\perp$ and b_z is computed numerically using a three-point formula for the numerical derivative. The HFB equations were solved using a second-order gradient method, which provides a fast convergence and allows for an arbitrary generalization of the numbers of constraints [38]. The main advantage of the computational scheme described above is that it has already been applied to several fission calculations using either the Gogny or the BCPM interactions [22,26–28,34,39], and its capability to describe the fission process is well constrained.

We have used the last version of the BCPM functional recently proposed to describe the physics of finite nuclei [31]. This functional has also proved to perform well in a series of calculations of fission properties including inner fission barrier heights, excitation energy of fission isomers, outer barrier heights, spontaneous fission lifetimes, etc. [34]. The idea behind the explicit form of the BCPM functional is to use a simple polynomial in the density to fit the energy per particle in both symmetric and neutron nuclear matter as obtained with state of the art many-body techniques and realistic nuclear interactions. The polynomial so obtained is used verbatim in finite nuclei but using the density of the finite nucleus instead. A standard contact spin-orbit term is added to reproduce magic numbers. Surface effects are considered by means of a finite range Gaussian interaction acting only in the direct channel. The Coulomb interaction is taken, as in many other calculations, exactly in the direct channel. The exchange Coulomb field is replaced by the Slater approximation and the repulsive contribution of the Coulomb interaction to the pairing channel is neglected. For the pairing interaction, a density-dependent pairing interaction has been used. One of the distinctive characteristics of the functional is its inclusion of the rotational energy correction (see below) to compute the ground-state binding energy. The rotational correction is also used in the fitting protocol in spite of the fact that its inclusion produces some artifacts near magic or semimagic nuclei [31]. They are a direct consequence of computing the rotational correction after variation and disappear if beyond mean-field effects such as configuration mixing of quadrupole deformed shapes are taken into account. Unfortunately, the artifacts in the rotational correction lead to spurious peaks in both the S_n, S_{2n} and related quantities near magic or semimagic nuclei, which can produce unphysical abundances in r-process calculations. For this reason, we have decided to remove the rotational correction in the evaluation of one and two neutron separation energies. The impact of this prescription in the S_n rms for $Z > 84$ is small increasing its value from 0.28–0.36 MeV. However, the rotational correction is maintained in fission barrier calculations as the artifacts do not appear in the relevant regions of the path to fission.

A. Spontaneous fission lifetimes, fission barriers, and collective inertias

We start defining the fission tunneling probability, P, from a state at excitation energy E_x through a transition state with an excitation energy ε on top of the fission barrier as:

$$P(E_x,\varepsilon) = \frac{1}{1 + \exp[2S(E_x,\varepsilon)]}. \tag{2}$$

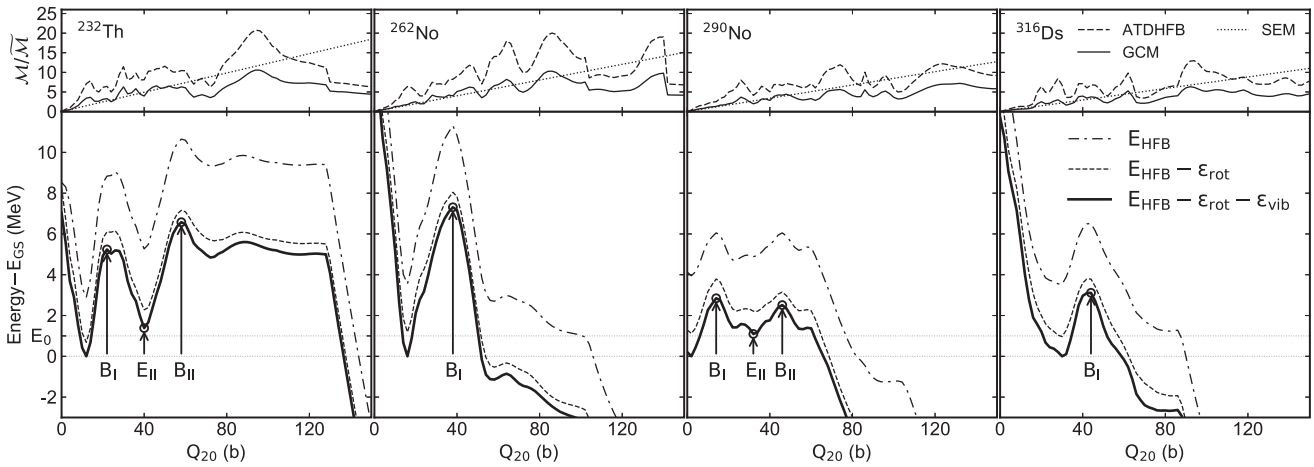

FIG. 1. Collective fission properties of ^{232}Th, ^{262}No, ^{290}No, and ^{316}Ds as a function of the quadrupole moment. Bottom panels show different contributions to the potential energy surface $\mathcal{V}(Q_{20})$ of Eq. (5). Top panels show collective inertias $\mathcal{M}(Q_{20})$ computed with the ATDHFB (dashed line), GCM (solid line), and semiempirical inertia formula (dotted line), renormalized to the reduced inertia $\widetilde{\mathcal{M}}$.

S is the integral action computed along the fission path, $L(Q_{20})$, between the classical turning points a and b:

$$S_L(E_x,\epsilon) = \int_a^b dQ_{20}\sqrt{2\mathcal{M}(Q_{20})[\mathcal{V}(Q_{20})+\varepsilon-(E_x+E_{\rm GS})]}, \tag{3}$$

where the fission path is obtained by minimizing the effective potential energy, $\mathcal{V}(Q_{20})$, (so-called static approach). In the case of spontaneous fission the excitation energy of the nucleus corresponds to the so-called collective ground-state energy, E_0, and the transition state is taken at zero excitation energy on top of the barrier. Hence, the spontaneous fission half-life ($t_{\rm sf}$) is given by the semiclassical Wentzel-Kramers-Brillouin (WKB) theory [40]:

$$t_{\rm sf} = \frac{\ln 2}{nP(E_0,0)} = \frac{2.86\times10^{-21}\ {\rm s}}{P(E_0,0)}, \tag{4}$$

with n the number of assaults of the nucleus on the fission barrier per unit time [41]. Equation (3) shows that the theoretical description of spontaneous fission is based in three main ingredients: the collective inertias $\mathcal{M}(Q_{20})$, the effective potential energy $\mathcal{V}(Q_{20})$, and the energy of the collective ground state E_0. The effective potential energy $\mathcal{V}(Q_{20})$ is obtained by subtracting the vibrational and rotational zero-point energies from the total HFB energy:

$$\mathcal{V}(Q_{20}) = E_{\rm HFB}(Q_{20}) - \epsilon_{\rm vib}(Q_{20}) - \epsilon_{\rm rot}(Q_{20}). \tag{5}$$

The HFB energy $E_{\rm HFB}$ is defined as the expectation value of the Routhian with constraining operators:

$$\hat{\mathcal{H}} = \hat{\mathcal{H}}_{\rm HFB} + \sum_{\nu=1,2}\lambda_\nu\hat{Q}_{\nu0} + \sum_{\tau=p,n}\lambda_\tau\hat{N}_\tau, \tag{6}$$

$\hat{\mathcal{H}}_{\rm HFB}$ being the HFB Hamiltonian, $\hat{N}_p(\hat{N}_n)$ the proton (neutron) number operator, λ_i the Lagrange multipliers, Q_{10} the center-of-mass constraint preventing spurious solutions arising from center-of-mass motion, and $\hat{Q}_{20}$:

$$\hat{Q}_{20} = \sum_i^A \hat{z}_i^2 - \frac{1}{2}\left(\hat{x}_i^2+\hat{y}_i^2\right). \tag{7}$$

The rotational energy correction $\epsilon_{\rm rot}(Q_{20})$ is related to the restoration of the rotational symmetry and is computed in terms of the Yoccoz moments of inertia using the phenomenological approach of Ref. [42]. This approach includes a correction to account for the approximations involved in the evaluation of the Yoccoz moment of inertia. Finally, the vibrational energy correction $\epsilon_{\rm vib}(Q_{20})$ takes into account for quantal fluctuations in the collective degree of freedom Q_{20}.

The bottom panels of Fig. 1 show the different contributions of Eq. (5) to the potential energy surface (PES) in four different nuclei. Clearly the major reduction to $\mathcal{V}(Q_{20})$ comes from the rotational correction $\epsilon_{\rm rot}(Q_{20})$, while the vibrational correction $\epsilon_{\rm vib}(Q_{20})$ produces a smaller, yet not constant, shift. We also show the inner, B_I, and outer, B_{II}, barrier and the isomer excitation energy, E_{II}, defined as illustrated in the figure.

The second ingredient needed for the calculation of the SF lifetimes are the collective inertias $\mathcal{M}(Q_{20})$. In the present work we evaluated $\mathcal{M}(Q_{20})$ and $\epsilon_{\rm vib}(Q_{20})$ following two different schemes within the perturbative cranking approximation: the adiabatic time-dependent HFB theory (ATDHFB) [43] and the Gaussian overlap approximation to the generator coordinate method (GOA-GCM) [44]:

$$\mathcal{M}_{\rm ATDHFB}(Q_{20}) = \frac{{\rm M}_{-3}}{2({\rm M}_{-1})^2}, \tag{8}$$

$$\mathcal{M}_{\rm GOAGCM}(Q_{20}) = \frac{({\rm M}_{-2})^2}{2({\rm M}_{-1})^3}. \tag{9}$$

The energy-weighted momentum ${\rm M}_{-n}(Q_{20})$ of the quadrupole generating field can be expressed in terms of the two-quasiparticle excitations $|\alpha\beta\rangle$:

$${\rm M}_{-n}(Q_{20}) = \sum_{\alpha>\beta}\frac{|\langle\alpha\beta|Q_{20}|0\rangle|^2}{(E_\alpha+E_\beta)^n}, \tag{10}$$

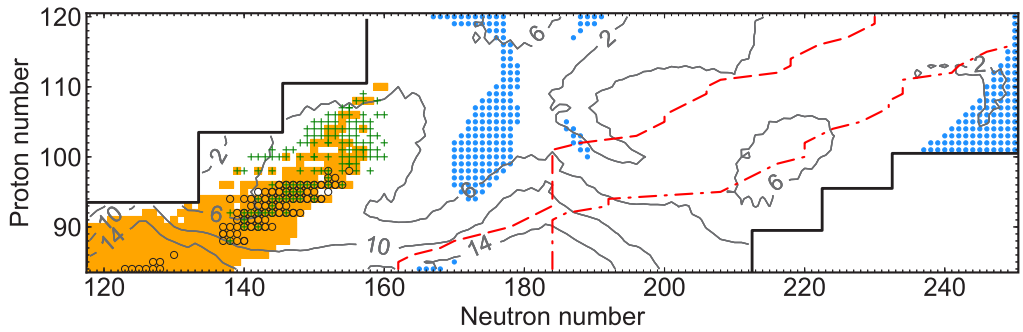

FIG. 2. Region of the nuclear landscape explored in this work. Nuclei present in the AME2012 mass table evaluation [46] are depicted with orange squares. Nuclei with experimentally measured fission barriers and spontaneous fission lifetimes are marked with open circles and crosses, respectively. Nuclei for which the BCPM interaction predicts an oblate-deformed ground state are depicted with solid circles. Dashed and dot-dashed lines represent the heaviest isotope of each element with $S_n \gtrsim 2$ and $S_n \gtrsim 0$ MeV, respectively. Contour lines show the highest predicted fission barrier, in MeV.

being $E_\alpha + E_\beta$ the excitation energy neglecting the quasiparticle-quasiparticle interaction. The ATDHFB scheme has the advantage that it naturally includes the time-odd response of the system to small perturbations in the deformation. In the simple case of a center-of-mass motion of the nucleus, the inclusion of the time-odd momenta allows the ATDHFB scheme to predict the exact collective inertia as the mass of the nucleus [44]. By contrast the GCM scheme does not include the time-odd response of the system and the inertias are underestimated unless time-odd momenta coordinates are used as collective degree of freedom. However, since translation and fission are collective phenomena involving different dynamics this argument cannot be used for claiming a superiority of the ATDHFB scheme over the GCM one.

The $\epsilon_{\rm vib}(Q_{20})$ energy is only defined in the GOA-GCM scheme [44]

$$\epsilon_{\rm vib}^{\rm GOAGCM}(Q_{20}) = \frac{G(Q_{20})}{\mathcal{M}_{\rm GOAGCM}}. \tag{11}$$

However, it is customary [30] to also introduce this quantity in the ATDHFB scheme by using the previous expression, but replacing the GOA-GCM inertia by the ATDHFB one:

$$\epsilon_{\rm vib}^{\rm ATDHFB}(Q_{20}) = \frac{G(Q_{20})}{\mathcal{M}_{\rm ATDHFB}}. \tag{12}$$

The quantity $G(Q_{20})$ is the overlap width between two configurations with similar quadrupole deformations:

$$G(Q_{20}) = \frac{\mathrm{M}_{-2}}{2(\mathrm{M}_{-1})^2}. \tag{13}$$

Several calculations of fission cross sections [16] use collective inertias based on the semiempirical parametrization $\mu = 0.054A^{5/3}$ MeV^{-1} and β_{20} as collective variable of the action integral (3). This expression reproduces experimental data in the actinide region for a particular choice of fission barriers [45]. Its validity for heavier nuclei and/or different barriers is questionable. Hence, we compare the spontaneous fission lifetimes obtained with this semiempirical expression with the results obtained using the ATDHFB and GOA-GCM approaches. Since the action integral is invariant under uniform scaling, and $\beta_{20} = \frac{\sqrt{20\pi}}{5A}\frac{Q_{20}}{r^2}$ with $r = 1.2A^{1/3}$ fm, we have that:

$$\mathcal{M}_{\rm SEMP} = \mu\left(\frac{d\beta_{20}}{dQ_{20}}\right)^2 = \frac{0.065}{A^{5/3}}\ \text{MeV}^{-1}\text{fm}^{-4}. \tag{14}$$

The top panels of Fig. 1 show the collective inertias obtained from ATDHFB, GCM, and the semiempirical schemes as a function of the quadrupole deformation. The values are normalized to the inertial mass that corresponds to the reduced mass of the fragments, m. Assuming pointlike fragments, it can be expressed as a function of the quadrupole moment as:

$$\widetilde{\mathcal{M}}(Q_{20}) = \frac{m}{\hbar^2}\left(\frac{dr}{dQ_{20}}\right)^2 = \frac{m_N}{4\hbar^2 Q_{20}}, \tag{15}$$

where $m_N = 938.919$ MeV$/c^2$ is the averaged nucleon mass. The fact that $\mathcal{M}_{\rm ATDHFB}$ and $\mathcal{M}_{\rm GOAGCM}$ are larger than $\widetilde{\mathcal{M}}$ suggests that the theoretical collective inertias are overestimated in our calculations, as we will discuss later in Sec. III A.

Figure 2 shows the region of the nuclear landscape explored in this work. Nuclei for which the BCPM interaction predicts a strong oblate deformation of the ground state ($\beta_{20} \leqslant -0.1$) are depicted with solid circles. These nuclei are supposed to undergo fission through a triaxial path and should be computed with an explicit breaking of the K quantum number. Since a triaxial code for the BCPM interaction is not currently available, we computed the axial path but it is necessary to keep in mind that predictions of the fission properties for these nuclei are less reliable.

B. Odd nuclei

The estimation of nuclear properties of nuclei with an odd number of protons and/or neutrons is a critical issue in SCMF models. A self-consistent solution obtained on the same footing as even-even nuclei is rather expensive from the computational point of view and therefore difficult to be implemented in systematic calculations (see, for example, Refs. [47,48] and references therein for a general comparison between different approaches). For this reason, a good compromise in systematic calculations is to use a phenomenological approach aimed to reproduce the experimental bulk nuclear properties of odd-even and odd-odd nuclei.

In this work, we computed the bulk nuclear properties of odd nuclei using the perturbative nucleon addition method (PNAM) [49]. By adopting the PNAM method BCPM maintains the same level of accuracy in the calculation of nuclear binding energies and fission properties for for even-even nuclei and odd-even and odd-odd nuclei. Namely, the BCPM EDF without rotational correction reproduces the experimental binding energies of even-even nuclei [46] with a rms deviation of 2.67 MeV, that decreases down to 2.37 MeV when odd nuclei computed with the PNAM are included. However, the agreement of the absolute binding energies can be misleading since the relevant quantities for r-process calculations are the neutron separation energies that determine the neutron capture cross sections. With the BCPM EDF the neutron separation energies S_n are reproduced with a rms deviation of 0.30 MeV for even-even nuclei and 0.36 MeV including odd and odd-odd nuclei. These results give us the confidence to explore the whole superheavy landscape using the BCPM EDF in combination with the PNAM.

Figure 3 shows the two-neutron separation energies S_{2n} predicted by BCPM for nuclei with $84 \leqslant Z \leqslant 120$ and the comparison with HFB21 [50] and FRDM [51] models. Jumps in the two-neutron separation energies, commonly defined as shell gaps $\Delta_{2n}(N) = S_{2n}(Z,N) - S_{2n}(Z,N+2)$, are usually associated with the presence of shell closures and during the r-process nucleosynthesis result in accumulation of matter. For example, for nuclei with $Z \sim 96$ the predicted neutron magic number $N = 184$ plays an important role in the production of the heaviest elements during the r-process nucleosynthesis in neutron star mergers, since it allows the accumulation of material around $A \sim 280$ [6]. Figure 4 shows that BCPM predicts a higher energy gap compared to HFB17 and FRDM for nuclei with $N = 184$ that smoothly disappears with increasing proton number. As we will discuss in Sec. III B this disappearance may allow the r path to proceeds towards heavier nuclei if the fission barriers around $^{284}_{100}$Fm are high enough.

For some nuclei BCPM predicts a potential energy surface with a vanishing fission barrier. For these nuclei a minimum energy cannot be defined and they are considered unstable, in the sense that after their production they will immediately decay by fission. They are followed by nuclei with a prolate ground state and depicted in Fig. 3 with a gap in the isotopic lines.

Regarding the collective inertias of odd nuclei, we applied the same perturbative scheme used for even-even nuclei described in Sec. II A. This approach neglects the enhancement of collective inertias due to the quenching of pairing correlations in systems with unpaired nucleons, leading to a possible underestimation of spontaneous fission lifetimes of nuclei with an odd number of neutrons and/or protons [28].

III. RESULTS

A. Benchmarks

In Ref. [34] we studied the fission properties of the BCPM EDF for a reduced set of even-even nuclei and compared our results with experimental measurements. In this paper we present the extension of such calculations to the whole superheavy landscape including nuclei with and odd number of protons and/or neutrons in the region $84 \leqslant Z \leqslant 120$ and $118 \leqslant N \leqslant 250$.

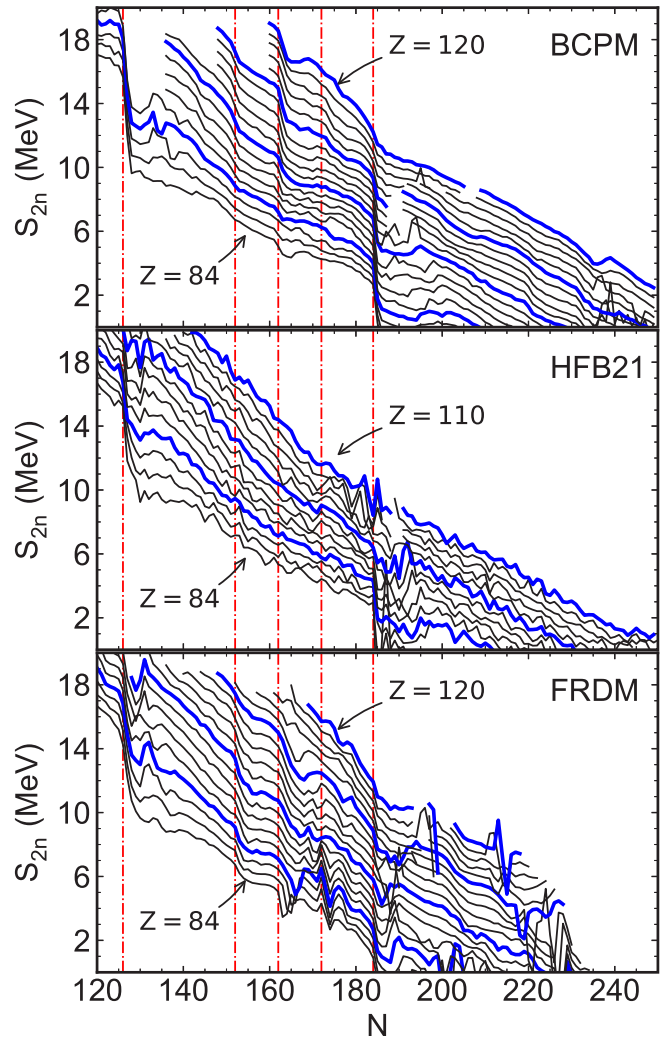

FIG. 3. Predicted two-neutron separation energies in MeV for nuclei with $84 \leqslant Z \leqslant 120$ as a function of neutron number for three different models: BCPM (top panel), HFB21 (middle panel), and FRDM (bottom panel). Isotopic chains are connected by solid lines. Nuclei with a proton number equal to 90, 100, 110, and 120 are depicted with blue thick lines.

In order to validate the theoretical predictions of the BCPM EDF, we compared our results of the barriers heights and isomer excitation energies with the available experimental data of Bjørnholm and Lynn [52] and Capote *et al.* [53]. Whether the fission barriers can be considered a physical observable or not is still a subject of discussion in the community. Without entering into this discussion, we would like to point out that experimental fission barriers are extracted from fission cross-section measurements, assuming nuclear level densities and shapes of the potential energy surface predicted by theoretical models. The experimental values of the fission barriers are therefore model dependent, and consequently the comparison with theoretical values should be taken with caution.

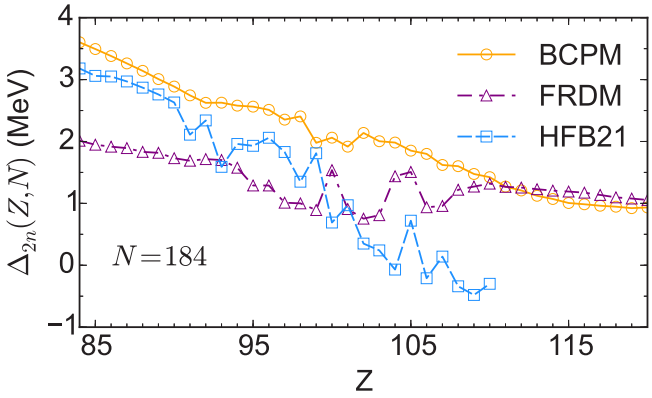

FIG. 4. Energy gap $\Delta_{2n} = S_{2n}(Z,N) - S_{2n}(Z,N+2)$ in MeV for nuclei with $N = 184$ as a function of proton number predicted by BCPM (open circles), FRDM (triangles), and HFB21 (squares).

Figure 5 shows the BCPM predictions and the experimental data of the inner (B_I) and outer (B_{II}) fission barrier height and the isomer excitation energy (E_{II}). We found that BCPM reproduces the B_I, B_{II}, and E_{II} experimental values of Bjørnholm and Lynn [52] with a rms deviation of 1.29, 0.81, and 1.22 MeV, respectively. The discrepancies with the data set of Capote *et al.* [53] are slightly larger: 1.51 MeV for

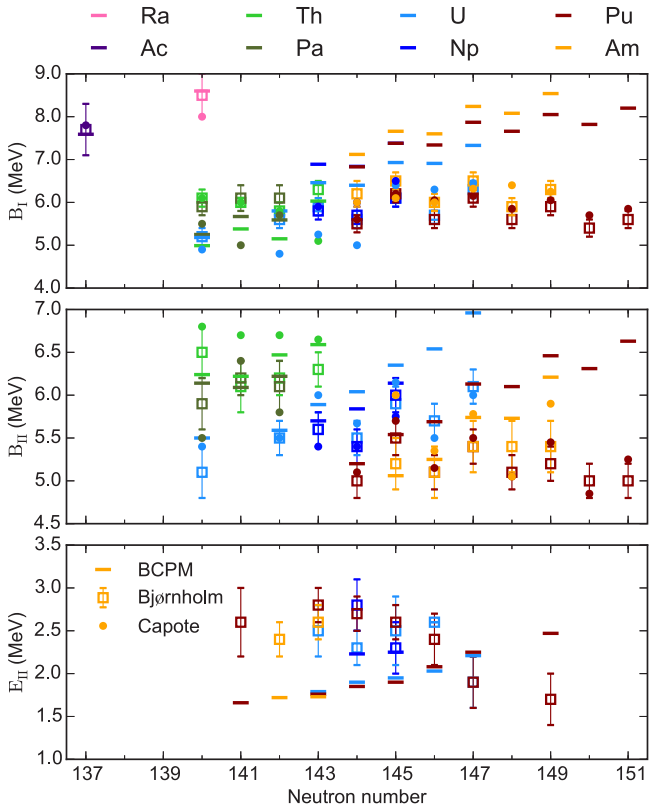

FIG. 5. Inner fission barrier height B_I (top panel), outer fission barrier height B_{II} (middle panel), and isomer excitation energy E_{II} (bottom panel) of eight isotopes computed with BCPM (lines) and compared with experimental data of Bjørnholm [52] (open squares) and Capote [53] (circles).

B_I and 0.97 MeV for B_{II}, while no data is available for E_{II}. The largest differences have been found in the uranium, plutonium, and americium isotopes. For these nuclei BCPM predicts an increase of the three quantities with increasing neutron number while experimental data shows an almost constant trend. Due to the imposition of axial symmetry the inner fission barrier heights are overestimated up to 2.5 MeV, which is in agreement with recent works studying the impact of triaxiality in fission calculations [19,20,26]. In many cases the PNAM provides a good description of the odd-even staggering of the fission barriers within single isotopic chains, and the inclusion of odd nuclei does not substantially modify the agreement with experimental data.

The other main spontaneous fission observable besides the barrier height is the spontaneous fission lifetime t_{sf}, which can be experimentally measured without any model assumption. This observable can be estimated with logarithmic precision within the semiclassical WKB formalism described in Sec. II A and is closely related to the penetration probability, an important ingredient in the evaluation of fission cross sections.

We computed the t_{sf} using the three different collective inertia schemes: ATDHFB [Eq. (8)], GCM [Eq. (9)], and the semiempirical formula [Eq. (14)]. Figure 6 shows the comparison between our results and the experimental data extracted from Refs. [54,55]. Both the ATDHFB and GCM microscopic schemes predict larger SF lifetimes compared to the experimental data, while the semiempirical formula overestimates the t_{sf} of nuclei with $Z \leqslant 98$ and slightly underestimates the lifetimes of nuclei with $Z \geqslant 99$. Due to the inclusion of the time-odd response of the nucleus to small perturbations of the deformation, the t_{sf} predicted by the ATDHFB scheme are systematically larger than the GCM ones.

Figure 6 shows that the spread among theoretical lifetimes and the discrepancy with experimental data are large for light actinides, while for heavier nuclei predictions become more accurate and precise. This convergence of theoretical calculations can be understood by looking at the fission barriers plotted in Fig. 1. The left panel shows the fission path of the nucleus ^{232}Th giving the largest difference between theoretical and experimental half-lives. This nucleus presents a broad fission barrier together with a large collective inertia, resulting in a large action integral $S(L)$ where variations in the collective inertias have a strong impact in the spontaneous fission lifetimes. On the other hand, the nucleus ^{262}No has a much shorter barrier with relatively small inertia between the classical turning points. This configuration reduces the value of the action integral and the impact of different collective inertia schemes in the absolute magnitude of t_{sf}, all giving a good prediction of the experimental value. For r-process nuclei where fission may play a relevant role, such as ^{290}No and ^{316}Ds plotted in Fig. 1, the t_{sf} has to be relatively short. Therefore these nuclei must have a narrow and/or low fission barrier and small collective inertias, bringing a level of precision in the estimation of the t_{sf} closer to the one obtained for the ^{262}No rather than the ^{232}Th.

For most of the isotopic chains the general trend of the spontaneous fission lifetimes is well reproduced by all the collective inertias schemes. Moreover, the odd-even staggering of the fission barriers is reflected in the lifetimes in a rather good

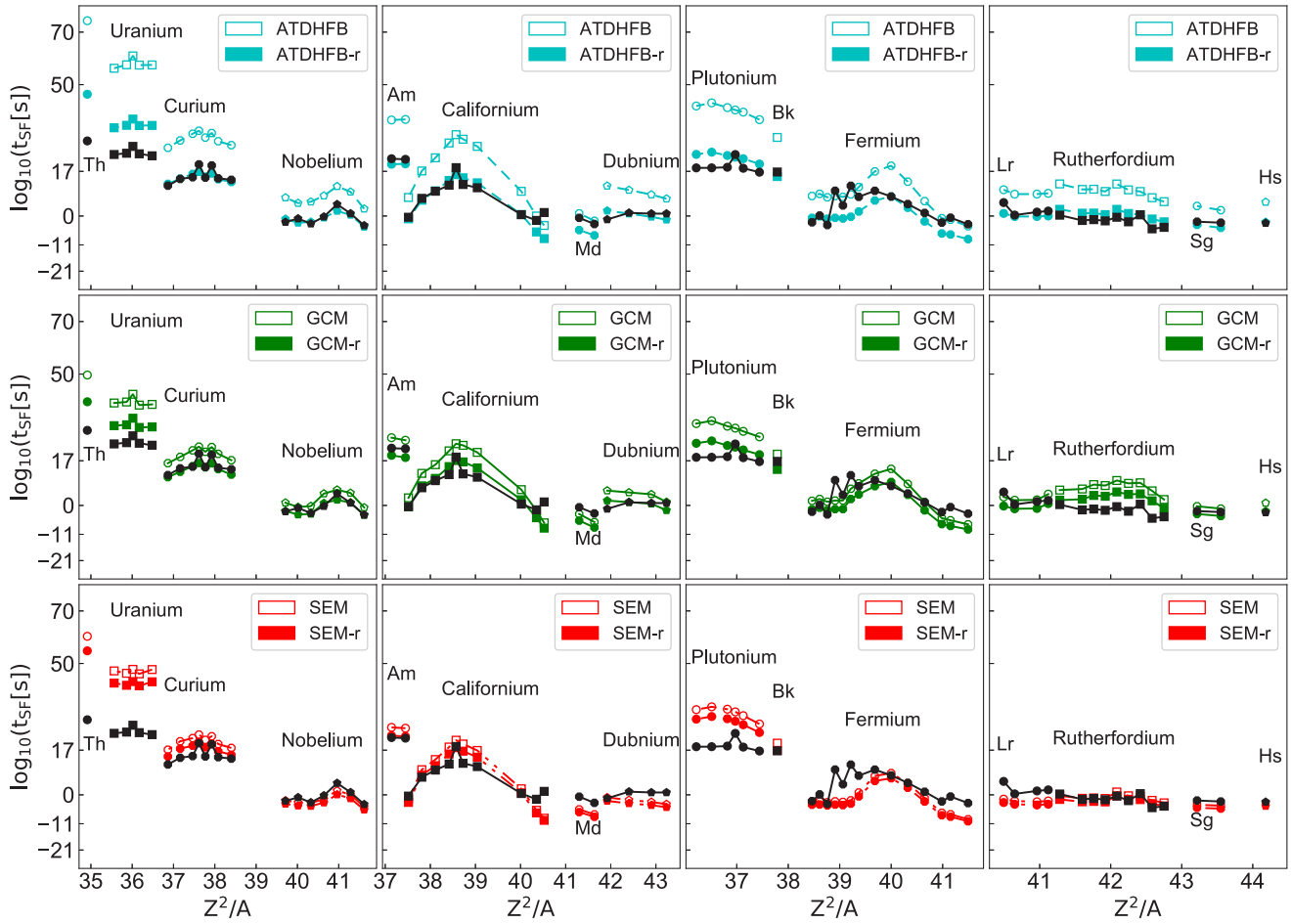

FIG. 6. Spontaneous fission lifetimes t_{sf} as a function of the fissibility parameter. Experimental data (black solid symbols) is compared with different inertia schemes: ATDHFB (top panels), GCM (middle panels), and semiempirical formula (bottom panels). The results obtained with the renormalized collective inertia (see Table I) are depicted with colored full symbols.

agreement with experimental data. However, it is important to notice that this staggering is more pronounced in the experimental t_{sf}, suggesting for a missing mechanism enhancing the collective inertias in these nuclei as discussed in Sec. II B.

The general overestimation of the spontaneous fission lifetimes in Fig. 6 suggests that both the fission barriers and the collective inertias are overestimated in our approach. We already traced back the overestimation of the fission barriers to the imposition of axial symmetry and in the following we will discuss the origin of the overestimation of the collective inertias in our calculations.

In this work the fission path was obtained as a function of the quadrupole moment by minimizing the potential energy (see Fig. 1). The simplicity of this scheme allows for a systematic calculation of fission properties through the whole superheavy landscape. However, it does not incorporate important dynamic effects that appear when the fission path is obtained by minimizing the collective action. As it was studied in several recent papers [35,36,39] the dynamic approach strongly reduces the collective inertia and the t_{sf}, improving the agreement with experimental data in actinides. Unfortunately such kinds of studies exploring multidimensional energy surfaces with several degrees of freedom are extremely expensive from a computational point of view and cannot be applied to systematic calculations like the one presented in this paper. Therefore we propose a renormalization of the collective inertias aimed to take into account the dynamics neglected in the static one-dimensional picture and improve the agreement with experimental data. The normalization coefficient is obtained by minimizing the deviation between theoretical calculations and experimental data of the spontaneous fission lifetimes for each scheme presented in Sec. II A. Since the t_{sf} can vary in many orders of magnitude, we follow the prescription of Ref. [56] and use the logarithm of the ratio of theory to experiment

$$R_\tau = \log\left(\frac{t_{\rm sf}^{\rm BCPM}}{t_{\rm sf}^{\rm exp}}\right). \tag{16}$$

The target performance $\bar{R}_\tau$ and the variance σ_τ are then obtained as:

$$\bar{R}_\tau = \frac{1}{N}\sum_{i=1}^{N} R_{\tau,i}, \tag{17}$$

$$\sigma_\tau = \frac{1}{N}\left(\sum_{i=1}^{N}(R_{\tau,i}-\bar{R}_\tau)^2\right)^{1/2}, \tag{18}$$

TABLE I. Target performances ($\bar{R}_\tau$) and variances (σ_τ) of the spontaneous fission lifetimes obtained with ATDHFB, GCM, and semiempirical collective inertias described in Sec. II A. The bottom table shows the results obtained by multiplying the collective inertias by a renormalization factor (0.497 for ATDHFB, 0.731 for GCM, and 0.868 for SEMP). Experimental values extracted from Ref. [54,55].

$\mathcal{M}$	$\bar{R}_\tau$	σ_τ
ATDHFB	11.583	6.447
GCM	4.691	4.236
SEMP	2.036	6.126
ATDHFB-r	−0.007	3.403
GCM-r	−0.006	3.339
SEMP-r	0.004	5.231

N being the number of nuclei used in the benchmark. Comparing the logarithm of the ratio of theory to experiment we found that the target performance of the ATDHFB, GCM, and semiempirical inertia schemes is 11.583, 4.691, and 2.036, respectively. We find that the minimum value of the target performance is obtained by multiplying the ATDHFB, GCM and SEMP collective inertias by a factor 0.497, 0.731, and 0.868, respectively (labeled as ATDHFB-r, GCM-r, and SEMP-r in Fig. 6 and Table I). Figure 6 shows that this renormalization strongly reduces the t_{sf} of light actinides (Th, U, and Pu), where the high stability against the fission process leads to large values of the action integral and larger discrepancies with the experimental data. On the other hand, as we move toward heavier nuclei the impact of the renormalization in t_{sf} tend to decrease. This is shown in Fig. 6 where the differences between nonrenormalized and renormalized t_{sf} are smaller for heavier nuclei as compared to lighter ones. The renormalization of the collective inertias, which is mostly justified by the inclusion of dynamic effects beyond static calculations, will be considered as an alternative to other approaches such as the renormalization of the fission barriers proposed in Ref. [16] aimed to improve the agreement between theoretical calculations and experimental data. Dynamic effects also tend to increase the rotational and vibrational corrections of Eq. (5) but to a much lesser extent than the effect on the inertias. This is the reason why only the inertias have been renormalized.

The results of the fission barrier height and the SF lifetimes presented in this section proved the capability of the BCPM+PNAM scheme to reproduce the experimental data. We consider this agreement rather satisfactory, especially taking into account that the BCPM EDF was fitted in order to reproduce the nuclear masses of the AME2003 mass table [57] and it does not contain any information regarding the fission properties of superheavy nuclei.

B. Systematic of fission barriers

Figure 7 shows the highest barrier predicted by the BCPM EDF for nuclei in the region $84 \leqslant Z \leqslant 120$ and $118 \leqslant N \leqslant 250$ and the comparison with the theoretical predictions of the FRLDM [13] and HFB-14 [16] nuclear models.

The general trend of fission barriers gives a crude estimation of the stability of nuclei against the fission process and reflects

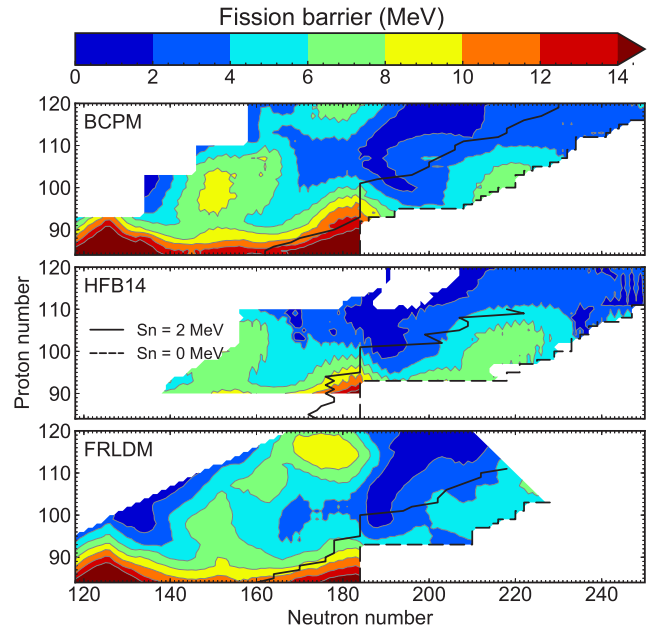

FIG. 7. Calculated fission barrier heights in MeV in the region $84 \leqslant Z \leqslant 120$ and $118 \leqslant N \leqslant 250$ for three different mass models: BCPM (this study, top panel), HFB14 [16] (middle panel), and FRLDM [13] (bottom panel). Drip lines are represented by dashed black lines. The solid black lines show the r-process path, given by the heaviest isotope of each nuclei with $S_n \geqslant 2$ MeV.

the impact of shell closures. BCPM predicts five different islands of local maximum placed around nuclei $^{210}_{84}$Po, $^{268}_{84}$Po, $^{250}_{100}$Fm, $^{320}_{102}$No, and $^{300}_{120}$Ubn. The increase of fission barriers around $^{210}_{84}$Po and $^{268}_{84}$Po is related with the presence of the neutron magic numbers $N = 126$ and $N = 184$, leading to spherical nuclei with fission barriers up to 24–25 MeV. These two islands are separated by prolate nuclei with fission barriers around 12 MeV and a group of slightly oblate nuclei around $Z/N = 86/176$. Regions around $^{250}_{100}$Fm and $^{300}_{120}$Ubn are usually referred to as the "peninsula of known nuclei" and "island of stability," respectively [58]. The peninsula is formed by prolate-deformed nuclei with fission barriers between 6 and 9 MeV and it extends up to $Z/N \approx 110/166$. On the other hand, nuclei in the island of stability are either oblate (for lower N) or spherical (higher N) with fission barriers around 7 MeV. The peninsula and the island are separated by a rather narrow region of prolate nuclei with $A \sim 280$ where the fission barriers decrease to 3–5 MeV. Finally, the region around $^{320}_{102}$No is formed by strongly deformed nuclei ($\beta_{20} \sim 0.25$) with barriers between 7 and 8 MeV. BCPM predicts a region of vanishing barriers around $Z/N = 116/208$ and for nuclei with $A \sim 292$ around $N \sim 188$. As discussed later, this region of vanishing barriers may play an important role for terminating the r process via neutron-induced fission.

For a complete comparison Fig. 7 shows the fission barriers predicted by two other models: the macroscopic-microscopic finite range liquid drop model (FRLDM) [13] and the self-consistent mean-field approach based on the HFB14 Skyrme parametrization [16]. Both models show a general trend of the fission barriers similar to the one obtained with the BCPM

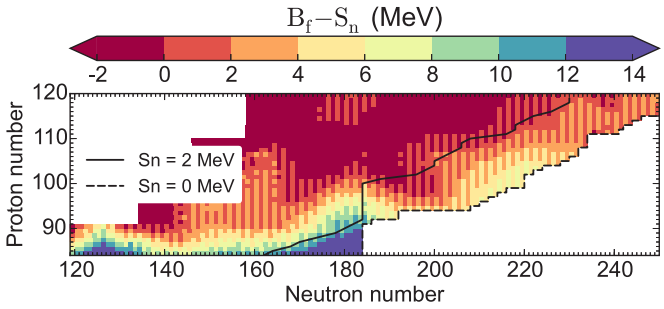

FIG. 8. Energy window for the neutron-induced fission $B_f - S_n$ computed with the BCPM EDF. The solid black line represents the r-process path, given by the heaviest isotope of each nuclei with $S_n \geqslant 2$ MeV. The drip line predicted by the BCPM EDF is represent by dashed line.

EDF, with two islands of larger fission barriers around $Z/N = 90/184$ and $Z/N = 100/150$. Moreover, all the models predict a region of vanishing barriers around $Z/N = 104/188$. BCPM tends to predict larger barriers compared to those obtained with FRLDM for nuclei with $Z \leqslant 100$ corresponding to the neutron magic number $N = 184$. On the other hand, FRLDM predicts larger barriers (up to 5 MeV) in the region around $Z/N = 112/178$. Comparing the results obtained with BCPM and HFB14, we found these two mean-field models predict similar maximum fission barrier heights. The rms deviation between both models is 1.03 MeV, while the deviation between BCPM and FRLDM is 2.31 MeV. The major differences between BCPM and HFB14 are found in neutron-rich actinides where HFB14 predicts fission barriers larger by 2–3 MeV, and around $Z/N = 97/187$ and $106/196$ where BCPM barriers are roughly 2 MeV larger. It is clear then, that different models predict quantitatively different fission barriers in the region far from stability where the r process occurs. However, it is not possible to determine *a priori* which model is the preferable one. Therefore, calculations of fission reaction rates obtained from different nuclear models are required to assess the sensitivity of the r-process abundances to uncertainties in the estimation of the fission properties of superheavy nuclei.

Another quantity of major interest for astrophysical calculations is the energy window for neutron-induced fission given as the difference between the highest fission barrier height and the neutron separation energy $B_f - S_n$. This quantity indicates whether the production of superheavy nuclei during the r process can be inhibited by neutron-induced fission, recycling the material to lighter fission products. Figure 8 shows the values of $B_f - S_n$ obtained with the BCPM EDF. In principle, an appropriate estimation of the r-process path would require a network calculation taking into account neutron captures, β decays, and photodissociations. However, from simple arguments it is still possible to make a rough estimation of where the r-process path will be terminated by the neutron-induced fission. For typical astrophysical conditions in neutron star mergers, the r-process path is supposed to proceed along nuclei with constant neutron separation energy $S_n \sim 2-3$ MeV [59]. On the other hand, the excitation energy of a nucleus after capturing a neutron is given by the neutron separation energy. From these arguments one concludes that nuclei with

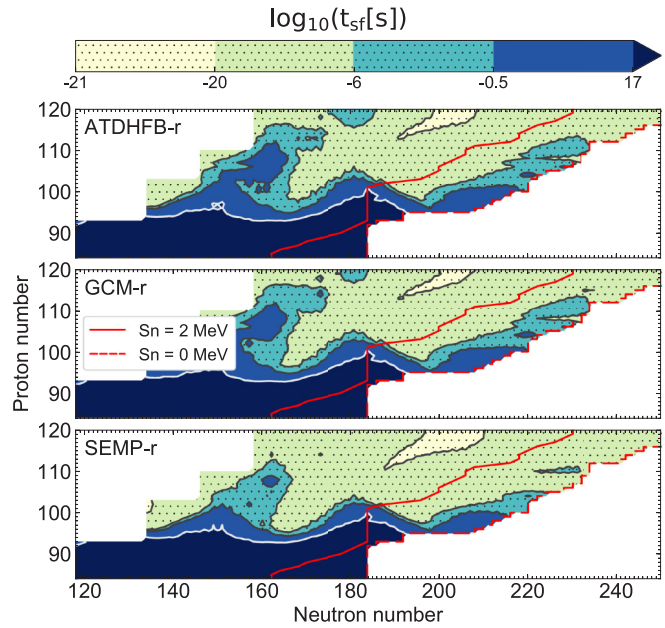

FIG. 9. Decimal logarithm of the spontaneous fission lifetimes computed with the ATDHFB-r (top panel), GCM-r (middle panel), and SEMP-r (bottom panel) schemes (see Table I for the renormalization coefficients). Dotted regions represent nuclei with $t_{sf} \leqslant 3$ s which may be relevant for r-process calculations. All the lifetimes were obtained with $E_0 = 0.5$ MeV.

$B_f - S_n \sim 2$ MeV will immediately fission after capturing a neutron [60,61]. Figure 8 shows how the r-process path is stacked along nuclei with $N = 184$ until $Z = 102$, where the disappearance of the jump in the neutron separation energy described in Sec. II B allows us to overcome the waiting point. However, at this point the r-process path has already proceeded into the region of low fission barriers where $B_f - S_n$ drops below zero ($Z/N = 102/190$). Therefore, we may expect the r-process nucleosynthesis of superheavy nuclei to be terminated by the neutron induced fission in the region around $Z/N = 102/190$.

C. Systematic of fission lifetimes

The trend of the fission barriers gives only a rough hint of the stability of the nucleus against the fission process. As it was already explained in Sec. II A, the probability of the system to penetrate the fission barrier is determined by a complex process where several ingredients must be taken into account and it can not be solely determined by the height of the barrier. A more complete picture can be therefore obtained studying the trend of the spontaneous fission lifetimes and the contribution of the different terms entering in Eq. (3). In this section we will study the sensitivity of the spontaneous fission lifetimes to variations in the collective inertias $\mathcal{M}(Q_{20})$, the vibrational energy corrections $\epsilon_{\rm vib}(Q_{20})$ and the collective ground-state energy E_0.

Figure 9 shows the $t_{\rm sf}$ obtained from Eq. (3) using the three different schemes of the collective inertias described in Sec. II A and renormalized using the coefficients of Sec. III A. For the ATDHFB and GCM schemes the vibrational energy

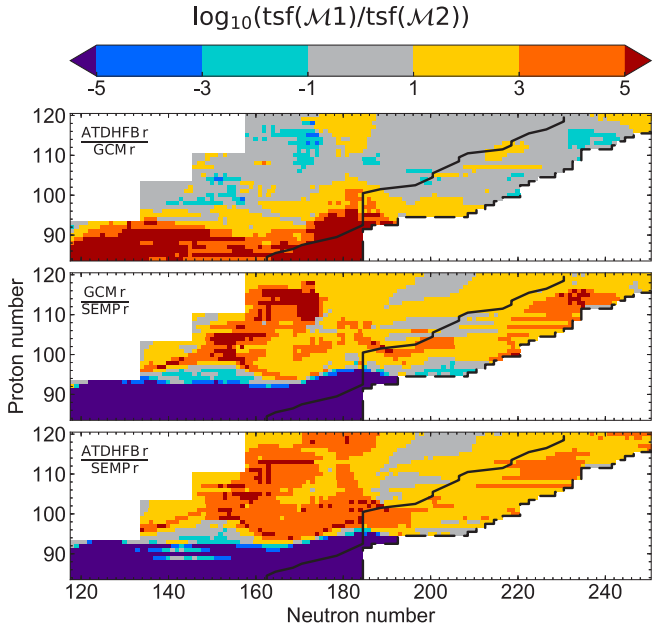

FIG. 10. Logarithm of the ratio of the spontaneous fission lifetimes for different combinations of collective inertias: $R^{\mathrm{ATDHFB}}_{\mathrm{GCM}}$ (top panel); $R^{\mathrm{GCM}}_{\mathrm{SEMP}}$ (middle panel), and $R^{\mathrm{ATDHFB}}_{\mathrm{SEMP}}$ (bottom panel).

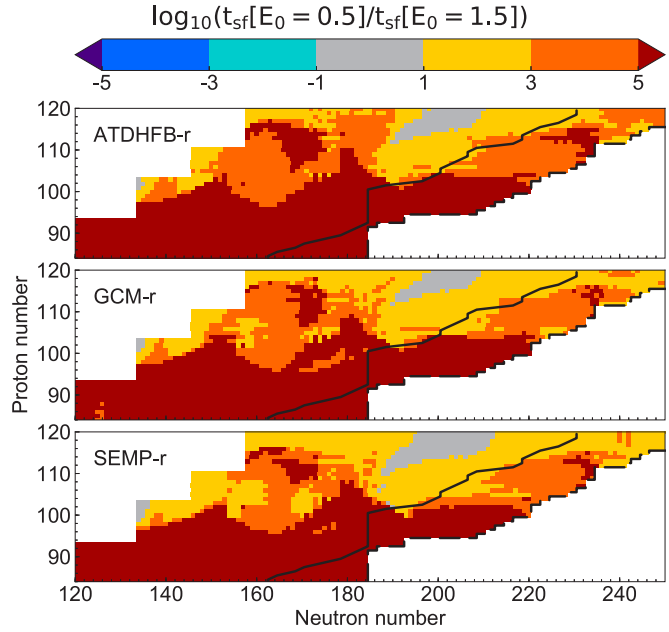

FIG. 11. Sensitivity of the spontaneous fission lifetimes to different values of the collective ground-state energy $\log_{10}[t_{\mathrm{sf}}(E_0 = 0.5\,\mathrm{MeV})/t_{\mathrm{sf}}(E_0 = 1.5\,\mathrm{MeV})]$ computed with different collective inertias: ATDHFB (top panels), GCM (middle panels), and semiempirical inertia formula (bottom panels).

corrections are consistently computed using Eqs. (12) and (11). For the semiempirical inertias we arbitrarily choose the $\epsilon^{\mathrm{GCM}}_{\mathrm{vib}}(Q_{20})$ scheme. Regarding the collective ground-state energy, all the lifetimes were obtained with $E_0 = 0.5$ MeV. Due to the arbitrariness in the choice of these last two parameters, the second part of this section will be devoted to study the sensitivity of the lifetimes on ϵ_{vib} and E_0.

From Fig. 9 it is possible to conclude that the trend of the spontaneous fission lifetimes resembles the general trend of the maximum fission barrier height plotted in the top panel of Fig. 7. This means that quantities such as collective inertias and the shape of the barrier are responsible for local variations in the stability of the nucleus against the fission process. The three schemes predict a region around $Z/N = 120/200$ with lifetimes of the order $t_{\mathrm{sf}} \sim 10^{-21}$ s, corresponding to nuclei with almost vanishing fission barriers.

For a more detailed comparison between the different models Fig. 10 shows the ratio of the lifetimes computed with different collective inertia schemes: ATDHFB to GCM (top panel), ATDHFB to semiempirical inertias (middle panel), and GCM to semiempirical inertias (bottom panel). The values showed in this plot correspond to the quantity

$$R^{\mathcal{M}1}_{\mathcal{M}2} = \log\left(\frac{t_{\mathrm{sf}}(\mathcal{M}_1)}{t_{\mathrm{sf}}(\mathcal{M}_2)}\right), \tag{19}$$

being $t_{\mathrm{sf}}(\mathcal{M}_i)$ the spontaneous fission lifetime computed using the collective inertia $\mathcal{M}_i$. Figure 10 shows that the largest variations among the different schemes are found in nuclei with $Z \lesssim 96$, where the spontaneous fission lifetimes are large. This is because in these nuclei differences in the collective inertia strongly impact the absolute value of the action integral $S(L)$ entering in the exponential of the lifetimes t_{sf}. In the r process we are interested in nuclei with $t_{\mathrm{sf}} \leqslant 3$ s (marked as the dotted region in Fig. 9), since this is the average time scale at which the r process operates from the onset of neutron captures till the exhaustion of all neutrons. Figure 10 shows that for these nuclei the variations in the t_{sf} predicted by the different collective inertia schemes are usually below three orders of magnitude, much lower than for the rest of the nuclei. By renormalizing the inertias we were able to reduce the sensitivity of the spontaneous fission lifetimes, especially in the case of the ATDHFB and GCM schemes. In the latter cases the difference for most of the r-process nuclei is less than one order of magnitude.

To better quantify the robustness of the spontaneous fission lifetimes Fig. 11 shows the sensitivity of t_{sf} to variations in the collective ground-state energy. We notice that by increasing E_0 by 1.0 MeV, the lifetimes can vary by more than five orders of magnitude even in nuclei with relatively short lifetimes and close to the r-process path. The reason is that nuclei with low barriers can still have a complex shape presenting multiple humps, such as the case of the ^{290}No plotted in Fig. 1. As it was already extensively studied in Ref. [22], the presence of a second fission isomer increases the spontaneous fission lifetimes by several orders of magnitude. By increasing the E_0 to 1.5 MeV the isomer can be shifted below the ground-state energy of the nucleus, and therefore the lifetimes are strongly reduced since the third hump does not contribute anymore to the penetration probability. Assuming that changes to E_0 have a similar impact in the action integral as the renormalization of the fission barrier, the latter may affect the location of the fissioning region for the r-process nucleosynthesis more than the renormalization of the collective inertias.

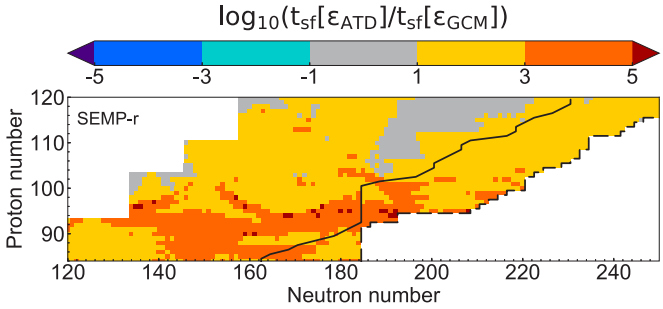

FIG. 12. Sensitivity of the spontaneous fission lifetimes to different values of the collective ground-state energy $\log_{10}[t_{sf}(\epsilon_{vib}^{ATDHFB})/t_{sf}(\epsilon_{vib}^{GCM})]$ computed using the semiempirical collective inertias.

For completeness we conclude this discussion studying the impact of the vibrational zero-point energy correction ϵ_{vib} on the spontaneous fission lifetimes. Figure 12 shows the logarithm of the ratio of t_{sf} computed with the same semiempirical inertias and two different ϵ_{vib} calculations, obtained from the ATDHFB and GCM formalisms of Eqs. (12) and (11). We found that the t_{sf} computed with the ATDHFB ϵ_{vib} are usually between 1 and 2 orders of magnitude larger than the GCM ones for r-process nuclei. This variation is similar to the one obtained for the collective inertias, in agreement with our conclusion that at short time scales the t_{sf} is more sensitive to the shape of the fission barrier.

D. α-decay half-lives

For completeness, we studied the competition between SF and α decay. The α-decay half-lives are obtained by means of the Viola-Seaborg formula [62] using the recent parametrization of Ref. [63]. The main advantage of the Viola-Seaborg formula is that it only requires the Q_α value of the parent nucleus to compute the α-decay half-lives. Comparing our predictions with the AME2012 atomic mass evaluation [46], we found that BCPM reproduces the Q_α values with a rms deviation of 0.68 MeV. For the α-decay half-lives of nuclei with $Z \geqslant 84$, the logarithm of the mean and standard deviations are 1.92 and 2.51, respectively, corresponding to deviations between theoretical half-lives and experimental data of factors 316 and 80. These large deviations in the t_α reflect the difficulties of reaching accuracies beyond the logarithmic precision in lifetimes calculations involving tunneling processes, as it was already mentioned in Sec. III A. Actually, the accuracy of the Viola-Seaborg formula itself is larger than a factor 6 [63], and it is important to notice that the deviations obtained in the t_α are smaller than those obtained in the t_{sf} without renormalization of the collective inertias.

Figure 13 shows the dominating channel (either SF or α decay) predicted by BCPM using different collective inertias, and the top panel shows the experimental data extracted from Ref. [46]. All the inertia schemes predict α decay to be the dominating channel in the region $84 \leqslant Z \leqslant 98$ and $118 \leqslant N \leqslant 156$, in good agreement with experimental data. The α-decay lifetimes seem to be overestimated around $Z/N = 102/150$ corresponding to a region of nuclei dominated by SF.

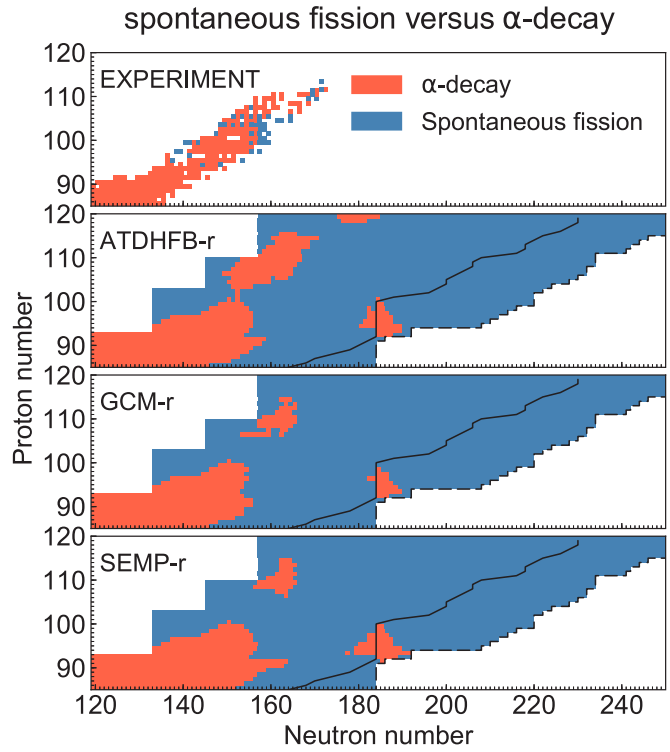

FIG. 13. Dominating channel between α decay and spontaneous fission for different collective inertias. For comparison, the top panel shows the dominating channel for nuclei experimentally observed [46].

One should also notice that the jumps in the neutron separation energy around the predicted magic neutron number $N = 184$ produces an island of nuclei dominated by α decay centered on $Z = 94$. Finally, the ATDHFB-r is the only scheme predicting the α decay to be the dominating channel for nuclei in the island of stability.

E. Neutron-induced rates

We conclude our study showing the impact of collective inertias on the calculations of rates relevant for r-process nucleosynthesis. Following the statistical picture described by the Hauser-Feshbach theory [64], for a target nucleus in the ground state the neutron-induced cross section for a reaction $i^{gs}(n,\text{out})$ can be written as [60]:

$$\sigma_{(n,\text{out})}^{gs} = \frac{\pi\hbar^2}{2mE_{cm}(2J_i^{gs}+1)(2J_n+1)} \times \sum_{J,\pi}(2J+1)\frac{T_n^{gs}(E,J^\pi,E_i^{gs},J_i^{gs},\pi_i^{gs})T_{out}(E,J^\pi)}{T_{tot}(E,J^\pi)}, \quad (20)$$

being m the reduced mass, E_{cm} the center-of-mass energy and $T(E,J^\pi)$ the transmission coefficient for a compound nucleus with energy E, spin J, and parity π. In the case of fission, the probability of the compound nucleus to penetrate all the possible fission barriers is mimicked by adding transition states on top of the saddle points. The fission transmission coefficient

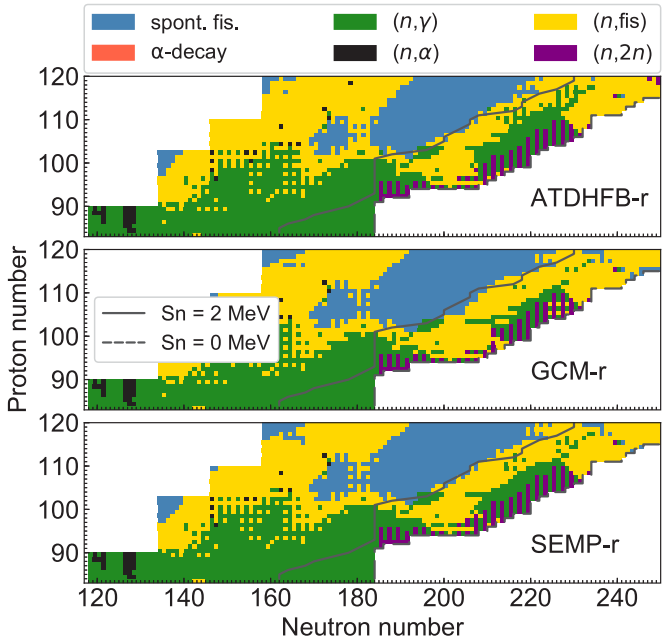

FIG. 14. Dominating decay channels: spontaneous fission, α-decay, neutron-capture, neutron-induced α emission, neutron-induced fission, and two-neutron emission computed using different collective inertias schemes.

$T_{\rm fiss}$ is thus given by [16]:

$$T_{\rm fiss}(E,J^{\pi}) = \int_0^E d\varepsilon\, P(E,\varepsilon)\rho(\varepsilon,J^{\pi}), \qquad (21)$$

with P defined in Eq. (2).

Nuclei in astrophysical plasma exist in both ground and excited states and the cross section of each excited state σ^x contributes to the final stellar cross section σ^* assuming that the relative population of the states follows a Maxwell-Boltzmann distribution. The stellar reaction rate for a given temperature T is then calculated by folding a Maxwell-Boltzmann distribution of relative velocities between projectiles and targets with the stellar cross section [65]:

$$\langle \sigma v\rangle_{(n,\rm out)} = \sqrt{\frac{8}{\pi m (kT)^3}} \times \int_0^{\infty} \sigma^*_{(n,\rm out)}(E) E \exp\left(-\frac{E}{kT}\right) dE. \qquad (22)$$

Using Eq. (22) we computed the neutron capture, neutron-induced fission, neutron-induced α decay, and neutron-induced two-neutron emission stellar rates over the whole superheavy landscape using the binding energies, fission barriers, and the renormalized collective inertias obtained from BCPM EDF. We adopted the level densities given by the constant temperature plus Fermi gas model and the Kopecky-Uhl generalized Lorentzian γ-ray strengths [53]. The calculations were carried out using the TALYS [66] reaction code for a range of temperatures between 0.01 and 10 GK [67]. Figure 14 shows the dominating decay channel of each nucleus for typical conditions of r process in neutron star mergers ($T = 0.9$ GK, $n_n = 1.0 \times 10^{28}$ cm^{-3}) [6]. Comparing the rates obtained from the different collective inertias we found that all the schemes predict a very similar scenario with fission dominating over the neutron capture for nuclei in the r-process path above the neutron magic number $N = 184$. There is a region above $N = 206$ where neutron capture is the dominating channel. However, the r-process path may never reach this corridor due to the large $(n,\rm fis)$ and $(n,2n)$ rates at lower N. We conclude then that independently of the computational scheme, the production of nuclei heavier than $N > 184$ will be strongly hindered due to the dominance of neutron-induced fission.

IV. CONCLUSIONS

We have presented fission properties of 3640 superheavy nuclei obtained within the self-consistent mean-field scheme and the BCPM EDF. The fission path is computed by minimizing the potential energy using the axial quadrupole moment operator as a collective degree of freedom and allowing for octupole and hexadecapole deformations. The potential energy surface of nuclei with an odd number of protons and/or neutrons is calculated using the PNAM, maintaining the level of accuracy obtained for even-even nuclei. The spontaneous fission lifetimes are evaluated using the WKB formula involving the effective potential, collective inertias and collective ground-state energy of the nucleus. Both vibrational and rotational corrections are properly subtracted from the effective potential. Collective inertias are evaluated using three different schemes (ATDHFB, GCM, and the semiempirical formula) to test the sensitivity of the spontaneous fission lifetimes.

Comparing our results with the available experimental data we found that BCPM tends to overestimate the spontaneous fission lifetimes, specially in the region of light actinides where the fission barriers and collective inertias are extremely large. In order to account for the effect of dynamic calculations in the determination of the fission path, we propose a phenomenological approach based on the renormalization of the collective inertias. By multiplying the collective inertias by a constant factor the agreement with experiment can be greatly improved. The comparison with experimental lifetimes showed that the accuracy and precision of the theoretical predictions improve as the mass number increases, providing the confidence to explore the region of nuclei relevant for the r process.

The landscape of the fission barrier obtained with the BCPM EDF show five islands of local maxima. Both the magic neutron numbers 126 and 184 lead to an increase of the fission barriers. Two other regions of enhanced barriers are found corresponding to the peninsula and island of stability. BCPM predicts a region of vanishing barriers for nuclei with $A \sim 292$, in agreement with other theoretical models. By studying the energy window of the neutron-induced fission, we concluded that the r-process path may terminate in this region and cycle to lighter fission products.

We performed a complete study of the sensitivity of the spontaneous fission lifetimes to the quantities entering in the WKB formula. We studied the variations on lifetimes when different schemes of the collective inertias, vibrational energy corrections, and collective ground-state energies are used. For

r-process nuclei, the renormalized collective inertia schemes result in variations of the spontaneous fission lifetimes smaller than three orders of magnitude and only one order of magnitude when GCM and ATDHFB alone are considered. We also found that the spontaneous fission lifetimes are strongly affected by the collective ground-state energy E_0. These large variations of the lifetimes can be related to a complex structure of the fission paths where several humps are present. Some of the barriers and isomers are placed 0.6–1.2 MeV above the ground state and their contribution to the action integral strongly depends on the value of E_0. Variations of the lifetimes on different schemes of the vibrational corrections confirmed the major role played by the fission barrier shape in the t_{sf} of r-process nuclei.

Finally, we studied the competition of fission with other channels. We computed the α-decay half-lives by means of the Viola-Seaborg formula and compared the results with the spontaneous fission lifetimes. We found that in all the schemes α decay dominates over spontaneous fission in nuclei with $Z \leqslant 98$ in good agreement with experimental data. Using the statistical approach we computed neutron-induced rates based on binding energies, fission barriers, and the nonrenormalized collective inertias obtained from the BCPM EDF. Our calculations showed that a proper treatment of the inertias should lead to rates that are rather insensitive to the different kind of inertias used, and that the synthesis of nuclei above $N > 184$ during the r process will be strongly inhibited by the neutron-induced fission.

The implementation of the BCPM rates in network calculations including a consistent evaluation of β delayed fission rates is necessary to determine the impact on r-process nucleosynthesis. Work along these lines is already in progress.

ACKNOWLEDGMENTS

The authors are grateful to Hans Feldmeier for his helpful discussions on theoretical aspects of the fission process, to Stephane Goriely for providing the HFB14 fission barriers plotted in Fig. 7, and to Zachary Matheson for carefully reading this manuscript. S.A.G. and G.M.P. acknowledge support from the Deutsche Forschungsgemeinschaft through contract SFB 1245, and the BMBF-Verbundforschungsprojekt No. 05P15RDFN1. The work of L.M.R. has been supported in part by the Spanish MINECO Grants No. FPA2012-34694 and No. FIS2012-34479 and by the ConsoliderIngenio 2010 Program MULTIDARK CSD2009-00064.

[1] J. J. Cowan, F.-K. Thielemann, and J. W. Truran, Phys. Rep. **208**, 267 (1991).
[2] G. Martínez-Pinedo, D. Mocelj, N. T. Zinner, A. Kelić-Heil, K. Langanke, I. V. Panov, B. Pfeiffer, T. Rauscher, K.-H. Schmidt, and F.-K. Thielemann, Prog. Part. Nucl. Phys. **59**, 199 (2007).
[3] S. Goriely, Eur. Phys. J. A **51**, 22 (2015).
[4] S. Goriely, J.-L. Sida, J.-F. Lemaître, S. Panebianco, N. Dubray, S. Hilaire, A. Bauswein, and H.-T. Janka, Phys. Rev. Lett. **111**, 242502 (2013).
[5] M. Eichler, A. Arcones, A. Kelic, O. Korobkin, K. Langanke, T. Marketin, G. Martínez-Pinedo, I. Panov, T. Rauscher, S. Rosswog, C. Winteler, N. T. Zinner, and F.-K. Thielemann, Astrophys. J. **808**, 30 (2015).
[6] J. J. Mendoza-Temis, M.-R. Wu, K. Langanke, G. Martínez-Pinedo, A. Bauswein, and H.-T. Janka, Phys. Rev. C **92**, 055805 (2015).
[7] L. Stavsetra, K. E. Gregorich, J. Dvorak, P. A. Ellison, I. Dragojević, M. A. Garcia, and H. Nitsche, Phys. Rev. Lett. **103**, 132502 (2009).
[8] C. E. Düllmann, M. Schädel, A. Yakushev, A. Türler, K. Eberhardt, J. V. Kratz, D. Ackermann, L.-L. Andersson, M. Block, W. Brüchle, J. Dvorak, H. G. Essel, P. A. Ellison, J. Even, J. M. Gates, A. Gorshkov, R. Graeger, K. E. Gregorich, W. Hartmann, R.-D. Herzberg, F. P. Heßberger, D. Hild, A. Hübner, E. Jäger, J. Khuyagbaatar, B. Kindler, J. Krier, N. Kurz, S. Lahiri, D. Liebe, B. Lommel, M. Maiti, H. Nitsche, J. P. Omtvedt, E. Parr, D. Rudolph, J. Runke, B. Schausten, E. Schimpf, A. Semchenkov, J. Steiner, P. Thörle-Pospiech, J. Uusitalo, M. Wegrzecki, and N. Wiehl, Phys. Rev. Lett. **104**, 252701 (2010).
[9] Y. T. Oganessian, F. S. Abdullin, C. Alexander, J. Binder, R. A. Boll, S. N. Dmitriev, J. Ezold, K. Felker, J. M. Gostic, R. K. Grzywacz, J. H. Hamilton, R. A. Henderson, M. G. Itkis, K. Miernik, D. Miller, K. J. Moody, A. N. Polyakov, A. V. Ramayya, J. B. Roberto, M. A. Ryabinin, K. P. Rykaczewski, R. N. Sagaidak, D. A. Shaughnessy, I. V. Shirokovsky, M. V. Shumeiko, M. A. Stoyer, N. J. Stoyer, V. G. Subbotin, A. M. Sukhov, Y. S. Tsyganov, V. K. Utyonkov, A. A. Voinov, and G. K. Vostokin, Phys. Rev. Lett. **109**, 162501 (2012).
[10] J. Khuyagbaatar, A. Yakushev, C. E. Düllmann, D. Ackermann, L.-L. Andersson, M. Asai, M. Block, R. A. Boll, H. Brand, D. M. Cox, M. Dasgupta, X. Derkx, A. Di Nitto, K. Eberhardt, J. Even, M. Evers, C. Fahlander, U. Forsberg, J. M. Gates, N. Gharibyan, P. Golubev, K. E. Gregorich, J. H. Hamilton, W. Hartmann, R.-D. Herzberg, F. P. Heßberger, D. J. Hinde, J. Hoffmann, R. Hollinger, A. Hübner, E. Jäger, B. Kindler, J. V. Kratz, J. Krier, N. Kurz, M. Laatiaoui, S. Lahiri, R. Lang, B. Lommel, M. Maiti, K. Miernik, S. Minami, A. Mistry, C. Mokry, H. Nitsche, J. P. Omtvedt, G. K. Pang, P. Papadakis, D. Renisch, J. Roberto, D. Rudolph, J. Runke, K. P. Rykaczewski, L. G. Sarmiento, M. Schädel, B. Schausten, A. Semchenkov, D. A. Shaughnessy, P. Steinegger, J. Steiner, E. E. Tereshatov, P. Thörle-Pospiech, K. Tinschert, T. Torres De Heidenreich, N. Trautmann, A. Türler, J. Uusitalo, D. E. Ward, M. Wegrzecki, N. Wiehl, S. M. Van Cleve, and V. Yakusheva, Phys. Rev. Lett. **112**, 172501 (2014).
[11] A. Baran, M. Kowal, P.-G. Reinhard, L. M. Robledo, A. Staszczak, and M. Warda, Nucl. Phys. A **944**, 442 (2015).
[12] P. Jachimowicz, M. Kowal, and J. Skalski, Phys. Rev. C **92**, 044306 (2015).
[13] P. Möller, A. J. Sierk, T. Ichikawa, A. Iwamoto, and M. R. Mumpower, Phys. Rev. C **91**, 024310 (2015).
[14] P. Jachimowicz, M. Kowal, and J. Skalski, Phys. Rev. C **95**, 014303 (2017).
[15] S. Goriely, M. Samyn, and J. M. Pearson, Phys. Rev. C **75**, 064312 (2007).
[16] S. Goriely, S. Hilaire, A. J. Koning, M. Sin, and R. Capote, Phys. Rev. C **79**, 024612 (2009).

[17] J. C. Pei, W. Nazarewicz, J. A. Sheikh, and A. K. Kerman, Phys. Rev. Lett. **102**, 192501 (2009).
[18] J. A. Sheikh, W. Nazarewicz, and J. C. Pei, Phys. Rev. C **80**, 011302 (2009).
[19] J. Erler, K. Langanke, H. P. Loens, G. Martínez-Pinedo, and P.-G. Reinhard, Phys. Rev. C **85**, 025802 (2012).
[20] A. Staszczak, A. Baran, and W. Nazarewicz, Phys. Rev. C **87**, 024320 (2013).
[21] J. Sadhukhan, W. Nazarewicz, and N. Schunck, Phys. Rev. C **93**, 011304 (2016).
[22] M. Warda, J. L. Egido, L. M. Robledo, and K. Pomorski, Phys. Rev. C **66**, 014310 (2002).
[23] M. Warda and L. M. Robledo, Phys. Rev. C **84**, 044608 (2011).
[24] J.-P. Delaroche, M. Girod, H. Goutte, and J. Libert, Nucl. Phys. A **771**, 103 (2006).
[25] M. Warda and J. L. Egido, Phys. Rev. C **86**, 014322 (2012).
[26] R. Rodríguez-Guzmán and L. M. Robledo, Phys. Rev. C **89**, 054310 (2014).
[27] R. Rodríguez-Guzmán and L. M. Robledo, Eur. Phys. J. A **50**, 142 (2014).
[28] R. Rodríguez-Guzmán and L. M. Robledo, Eur. Phys. J. A **52**, 12 (2016).
[29] B.-N. Lu, J. Zhao, E.-G. Zhao, and S.-G. Zhou, Phys. Rev. C **89**, 014323 (2014).
[30] N. Schunck and L. M. Robledo, Reports Prog. Phys. **79**, 116301 (2016).
[31] M. Baldo, L. M. Robledo, P. Schuck, and X. Viñas, Phys. Rev. C **87**, 064305 (2013).
[32] S. Goriely and G. M. Pinedo, Nucl. Phys. A **944**, 158 (2015).
[33] M. Bender, P.-H. Heenen, and P.-G. Reinhard, Rev. Mod. Phys. **75**, 121 (2003).
[34] S. A. Giuliani and L. M. Robledo, Phys. Rev. C **88**, 054325 (2013).
[35] J. Sadhukhan, J. Dobaczewski, W. Nazarewicz, J. A. Sheikh, and A. Baran, Phys. Rev. C **90**, 061304 (2014).
[36] J. Zhao, B.-N. Lu, T. Nikšić, D. Vretenar, and S.-G. Zhou, Phys. Rev. C **93**, 044315 (2016).
[37] A. Arzhanov, T. R. Rodríguez, and G. Martínez-Pinedo, Phys. Rev. C **94**, 054319 (2016).
[38] L. M. Robledo and G. F. Bertsch, Phys. Rev. C **84**, 014312 (2011).
[39] S. A. Giuliani, L. M. Robledo, and R. Rodríguez-Guzmán, Phys. Rev. C **90**, 054311 (2014).
[40] M. Brack, J. Damgaard, A. Jensen, H. Pauli, V. Strutinsky, C. Wong, and A. S. Jen, Rev. Mod. Phys. **44**, 320 (1972).
[41] A. Baran, K. Pomorski, A. Lukasiak, and A. Sobiczewski, Nucl. Phys. A **361**, 83 (1981).
[42] J. L. Egido and L. M. Robledo, in *Extended Density Functionals in Nuclear Structure Physics* (Springer, Berlin, 2004), Vol. 641, pp. 269–302.
[43] M. Girod and B. Grammaticos, Nucl. Phys. A **330**, 40 (1979).
[44] P. Ring and P. Schuck, *The nuclear many-body problem* (Springer-Verlag, New York, 1980).
[45] S. G. Nilsson, J. R. Nix, A. Sobiczewski, Z. Szymański, S. Wycech, C. Gustafson, and P. Möller, Nucl. Phys. A **115**, 545 (1968).
[46] M. Wang, G. Audi, A. H. Wapstra, F. Kondev, M. MacCormick, X. Xu, and B. Pfeiffer, Chinese Phys. C **36**, 1603 (2012).
[47] N. Schunck, J. Dobaczewski, J. McDonnell, J. Moré, W. Nazarewicz, J. Sarich, and M. V. Stoitsov, Phys. Rev. C **81**, 024316 (2010).
[48] L. M. Robledo, R. Bernard, and G. F. Bertsch, Phys. Rev. C **86**, 064313 (2012).
[49] T. Duguet, P. Bonche, P.-H. Heenen, and J. Meyer, Phys. Rev. C **65**, 014310 (2001).
[50] S. Goriely, N. Chamel, and J. M. Pearson, Phys. Rev. C **82**, 035804 (2010).
[51] P. Möller, J. R. Nix, W. Myers, and W. Swiatecki, At. Data Nucl. Data Tables **59**, 185 (1995).
[52] S. Bjørnholm and J. E. Lynn, Rev. Mod. Phys. **52**, 725 (1980).
[53] R. Capote, M. Herman, P. Obložinský, P. G. Young, S. Goriely, T. Belgya, V. Ignatyuk, A. J. Koning, S. Hilaire, V. Plujko, M. Avrigeanu, O. Bersillon, M. B. Chadwick, T. Fukahori, Z. Ge, Y. Han, S. Kailas, J. Kopecky, V. M. Maslov, G. Reffo, M. Sin, E. Soukhovitskii, and P. Talou, Nucl. Data Sheets **110**, 3107 (2009).
[54] N. E. Holden and D. C. Hoffman, Pure Appl. Chem. **72**, 1525 (2000).
[55] J. Khuyagbaatar, S. Hofmann, F. P. Heßberger, D. Ackermann, H. G. Burkhard, S. Heinz, B. Kindler, I. Kojouharov, B. Lommel, R. Mann, J. Maurer, K. Nishio, and Y. Novikov, Eur. Phys. J. A **37**, 177 (2008).
[56] G. F. Bertsch, W. Loveland, W. Nazarewicz, and P. Talou, J. Phys. G Nucl. Part. Phys. **42**, 077001 (2015).
[57] G. Audi, A. H. Wapstra, and C. Thibault, Nucl. Phys. A **729**, 337 (2003).
[58] P. R. Chowdhury, C. Samanta, and D. N. Basu, Phys. Rev. C **77**, 044603 (2008).
[59] G. Martínez-Pinedo, Eur. Phys. J. Spec. Top. **156**, 123 (2008).
[60] I. V. Panov, I. Y. Korneev, T. Rauscher, G. Martínez-Pinedo, A. Kelić-Heil, N. T. Zinner, and F.-K. Thielemann, Astron. Astrophys. **513**, A61 (2010).
[61] I. Petermann, K. Langanke, G. Martínez-Pinedo, I. V. Panov, P.-G. Reinhard, and F.-K. Thielemann, Eur. Phys. J. A **48**, 122 (2012).
[62] V. Viola and G. Seaborg, J. Inorg. Nucl. Chem. **28**, 741 (1966).
[63] T. Dong and Z. Ren, Eur. Phys. J. A **26**, 69 (2005).
[64] W. Hauser and H. Feshbach, Phys. Rev. **87**, 366 (1952).
[65] W. A. Fowler, Q. J. Roy. Astron. Soc. **15**, 82 (1974).
[66] http://www.talys.eu/.
[67] A. J. Koning, S. Hilaire, and S. Goriely, TALYS 1.8 user manual, 2015.